

Reverse flows and flattening of a submerged jet under the action of a transverse magnetic field

Abdellah Kharicha ^{1,*} Alexander Vakhrushev,¹ E. Karimi-Sibaki,¹ M. Wu,² and A. Ludwig²

¹*Christian-Doppler Lab for Metallurgical Applications of Magnetohydrodynamics,
Franz-Josef-Strasse 18, A-8700 Leoben, Austria*

²*Chair of Simulation and Modeling of Metallurgical Processes, Montanuniversitaet,
Franz Josef-StraÙe 18, A-8700 Leoben, Austria*



(Received 22 June 2021; accepted 18 October 2021; published 9 December 2021)

Spatial evolution of electrically conducting submerged jet flow is studied by numerical simulations for the case of a transverse uniform magnetic field. This situation occurs frequently in metallurgical industry where permanent magnetic fields are applied to control the liquid metal jets. We investigate through numerical simulations the flow characteristics for Reynolds ($Re < 4500$) and for moderate interaction numbers ($N < 0.1$). The results show the occurrence of far more complex phenomena than the expected magnetohydrodynamics damping effect, in agreement with many of the theoretical predictions made by Davidson [*J. Fluid Mech.* **299**, 153 (2001)]. The Lorentz force indeed acts against the flow within the main jet; however, it simultaneously accelerates the flow in adjacent quiescent regions. It results in a momentum redistribution in the form of a jet flattening in the direction of the applied magnetic field. Adjacent to the main jet, two strong reverse jets develop. The closure of induced currents is found to be responsible for these effects. While small-scale turbulent fluctuations are indeed suppressed, large coherent vortices aligned with the magnetic field develop within the shear region at the boundary between the main jet and the adjacent reverse jets.

DOI: [10.1103/PhysRevFluids.6.123701](https://doi.org/10.1103/PhysRevFluids.6.123701)

I. INTRODUCTION

The formation and evolution of jets under the influence of magnetic fields is one of the most important problems in modern astrophysics [1]. As an example, it is currently believed that cosmic gamma-ray bursts might possibly be the result of explosion where thin jets are formed. From a magnetohydrodynamics (MHD) point of view, these flows are generally characterized by very high magnetic Reynolds numbers (Rm) which represent the ratio between the advection to the diffusive flux of the magnetic fields. On much smaller scales, MHD effects on fluid jets are also an important topic in nuclear fusion blankets and in metallurgy [2–7]. However only few theoretical and experimental investigations of submerged jets can be found in literature [8–14]. In the case of axial magnetic fields, Krasnov *et al.* [13] have shown the jet to spread at much larger distances than without field. The reason lies in the fact that only turbulent fluctuations of the flow are influenced and suppressed by the presence of an axial field. In addition, transition to turbulence was delayed due to the stabilizing effect of the magnetic field. At strong magnetic fields, the jet profile becomes unsteady due to the development of traveling waves generated by the interaction of secondary radial flows and magnetic field.

*abdellah.kharicha@unileoben.ac.at

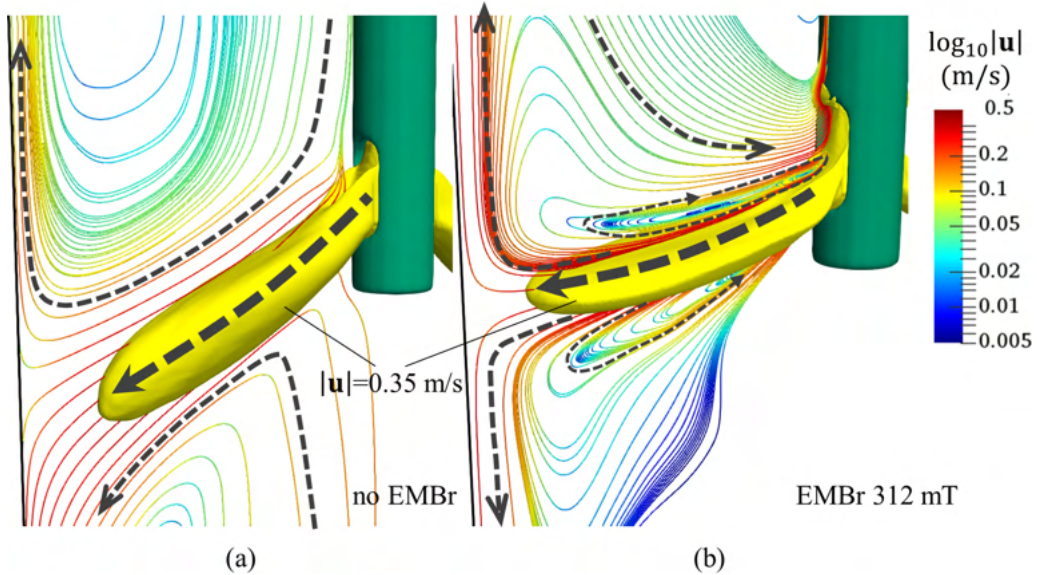


FIG. 1. Flow at the submerged entry nozzle in a continuous casting process. Jet flow structure (a) with and (b) without electromagnetic brake (EMBr). In (b), the development of two strong reverse-flow regions adjacent to the main jet are clearly visible [6].

Compared to axial fields, the influence of transverse fields has attracted significantly more attention especially in the field of application of electromagnetic brake in continuous casting [3–6]. In continuous casting, liquid metal flows are fed into the mold in the form of submerged jets that generate strong turbulences with large coherent vortices. Static transverse magnetic fields are used to damp the jet main flow and turbulence. Timmel *et al.* [3] experimentally investigated the impact of a DC magnetic field on the outlet flow from the submerged entry nozzle. It was found that applying a static magnetic field may destabilize the flow in a continuous caster. The flow measurements did not confirm the general belief of a reduction of the velocity fluctuations due to the presence of a transverse magnetic field. An important target in continuous casting is to keep the top free surface (known as meniscus) quiescent and to avoid the entrainment of nonmetallic inclusions in the solidifying region. However, industrial trials showed that not all magnitudes and positions of magnetic field resulted in better quality of metals. Against expectation, observations of the flow at free-surface meniscus was found to be accelerated rather than damped. To clarify the physical mechanisms, a large number of numerical and industrial investigations were undertaken in the last years [4–6]. These investigations have shown the occurrence of subtle MHD effects in industrial processes, such as rise of 2D turbulent flows and the importance of nonuniformity of the magnetic field on dynamics [15–17].

To our knowledge, Davidson [14] was the first to perform a theoretical analysis for low magnetic Reynolds numbers. He showed two important phenomena: (i) the jet develops a long thin sheetlike structure along the magnetic field direction, and (ii) the occurrence of reverse flows. Continuous casting investigations using mercury [18] as well as Large eddy simulations (LES) simulations of industrial flows [6] supported the existence of these reverse flows (Fig. 1). For some range of magnetic fields, instead of a damping effect these phenomena were associated with a deleterious strengthening of the flow at the meniscus level [5,6]. However, no mention of thin sheetlike structure can be found in these references, probably because of small dimensions in the magnetic field direction.

To further explore the topic, the present paper will undertake numerical simulations on a simpler geometry than that of a continuous casting process. A parametric study will be performed on a

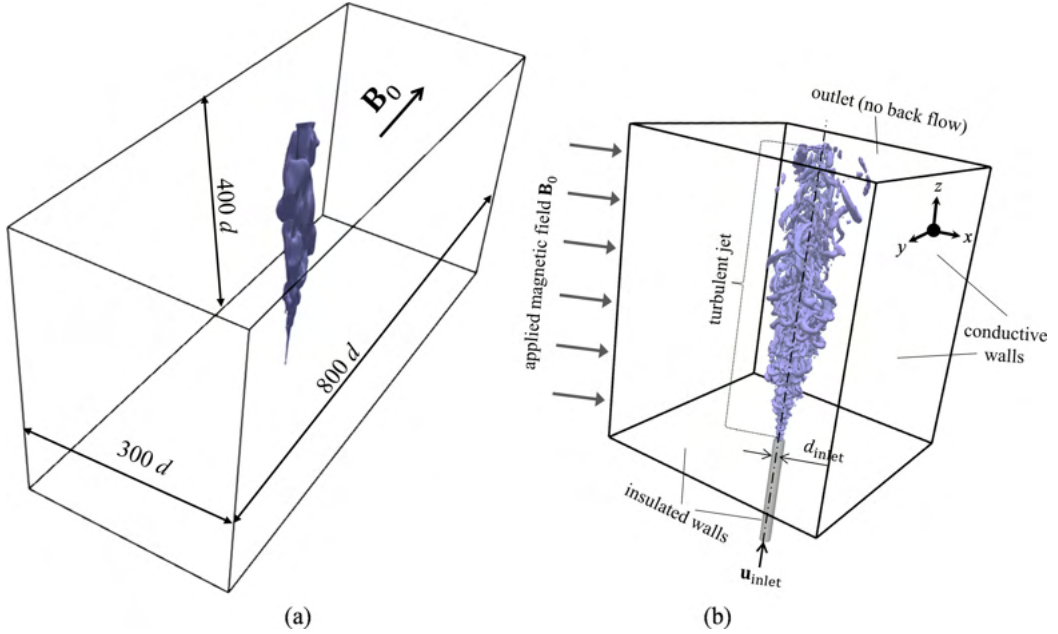


FIG. 2. Simulation domain: (a) overview of the actual geometry; (b) schematic setup for the numerical benchmark with boundary conditions. The jet flow direction is in the upward direction.

benchmark geometry inspired by the Davidson theoretical study [14] at moderate interaction and Hartmann numbers.

II. NUMERICAL MODEL AND GEOMETRY

The simulation setup schematic is shown in Fig. 2; the liquid is injected via a long tube into a domain which is bounded by a solid wall from the bottom part and has opened boundaries elsewhere. The outer boundaries defining the size of the opened domain are significantly remote from the jet inlet to avoid boundary effects; additionally, in the outlet back flow is restricted to avoid the numerical instabilities.

A homogeneous transverse magnetic field magnetic field $\mathbf{B}_0 = \{0 \quad B_0 \quad 0\}^T$ is applied in the domain.

The domain size was selected so that the walls are sufficiently far from the inlet of the jet to not influence the flow pattern. It is 400 inlet diameters in the vertical direction and 300 in the direction normal to the applied magnetic field. In the magnetic field direction, the domain size is extended up to 800 diameters since the jet will flatten and strongly extend in the field direction (which will be shown later in the results). The inlet long tube has a length of 15 inlet diameters.

Assuming the constant density ρ and laminar viscosity μ , the continuity and Navier-Stokes equations are

$$\nabla \cdot \mathbf{u} = 0, \quad (1)$$

$$\frac{\partial \mathbf{u}}{\partial t} + \nabla \cdot (\mathbf{u} \otimes \mathbf{u}) = \nu \nabla^2 \mathbf{u} - \nabla \cdot \boldsymbol{\tau}_{\text{SGS}} - \frac{1}{\rho} \nabla p + \frac{1}{\rho} \mathbf{j} \times \mathbf{B}, \quad (2)$$

where $\nu = \mu/\rho$ corresponds to kinematic viscosity and the operator $\nabla^2(\dots) \equiv \nabla \cdot \nabla(\dots)$ regards to a Laplacian. Please also note that the convective term in momentum equation (2) is taken in the conservative form by plugging the continuity equation (1) into substantial derivative since such

a formulation is preferable for the numerical discretization practice. The last term on the right represents the Lorentz force, where \mathbf{j} is the induced electric current obtained from Ohm's law:

$$\mathbf{j} = \sigma \cdot (-\nabla\varphi + \mathbf{u} \times \mathbf{B}), \quad (3)$$

where σ and φ are the electrical conductivity and potential. The conservation of the induced current ($\nabla \bullet \mathbf{j} = 0$) gives the equation for the electric potential:

$$\nabla \bullet (\sigma \nabla\varphi) = \nabla \bullet (\sigma \cdot (\mathbf{u} \times \mathbf{B})). \quad (4)$$

The subgrid-scale (SGS) Reynolds stress tensor τ_{SGS} is calculated using the wall-adapting local eddy-viscosity (WALE) turbulence model. WALE [19] is robust for the complex geometries with strong mesh refinements, and it is capable of predicting the formation of the turbulent structures coherent to the applied magnetic field [20,21].

To estimate the SGS stress tensor τ_{SGS} the following form is used:

$$\tau_{\text{SGS}} = -2 \cdot C_{\text{SGS}} \cdot (\Delta_{\text{SGS}})^2 \cdot |\mathbf{D}| \cdot \mathbf{D}, \quad (5)$$

where the norm of the strain rate tensor is defined as follows:

$$|\mathbf{D}| = \sqrt{2\mathbf{D} : \mathbf{D}}. \quad (6)$$

C_{SGS} and Δ_{SGS} are the model parameter and the filter width, respectively.

To make the equations dimensionless all variables as velocity $\mathbf{u} = \{u_x \ u_y \ u_z\}^T$, space coordinates $\mathbf{x} = \{x \ y \ z\}^T$, and integration time t are normalized based on the characteristic jet velocity U_0 and the inlet diameter as a characteristic length L_0 : $\hat{\mathbf{u}} = \frac{\mathbf{u}}{U_0}$, $\hat{\mathbf{x}} = \frac{\mathbf{x}}{L_0}$, $\hat{t} = \frac{t}{L_0/U_0}$. In the present study, the magnetic Reynolds number $Rm = |\mathbf{U}_0| \cdot L_0 \cdot \mu_0 \sigma$ is low (μ_0 is the magnetic vacuum permeability) and the induced magnetic field can be neglected, $\mathbf{B} \sim \mathbf{B}_0$.

The resulting dimensionless equations become

$$\frac{\partial \hat{\mathbf{u}}}{\partial \hat{t}} + \nabla \bullet (\hat{\mathbf{u}} \otimes \hat{\mathbf{u}}) = -\nabla \hat{p} + \frac{1}{\mathcal{R}e} \Delta^2 \hat{\mathbf{u}} - \nabla \bullet \hat{\tau}_{\text{SGS}} + \frac{\mathcal{H}a^2}{\mathcal{R}e} ((-\nabla \hat{\varphi} + \hat{\mathbf{u}} \times \hat{\mathbf{B}}) \times \hat{\mathbf{B}}), \quad (7)$$

$$\nabla^2 \hat{\varphi} = \nabla \bullet (\hat{\mathbf{u}} \times \hat{\mathbf{B}}). \quad (8)$$

The jet MHD flow is characterized by two nondimensional parameters, the Reynolds Re and Hartmann $\mathcal{H}a$ numbers. The Hartmann number represents the ratio of the Lorentz to the viscous force:

$$\mathcal{H}a = |\mathbf{B}_0| \cdot L_0 \cdot \sqrt{\sigma/\rho \cdot \nu}. \quad (9)$$

This number appears in combination of the Reynolds number, within the so-called interaction number:

$$\mathcal{N} = \frac{\mathcal{H}a^2}{\mathcal{R}e} = \frac{L_0}{U_0} \cdot \frac{\sigma_0 |\mathbf{B}_0|^2}{\rho} = \frac{t_{\text{adv}}}{\tau}, \quad (10)$$

which represents the ratio between the characteristic advection time t_{adv} to the Joule damping time τ . The bottom horizontal wall is electrically insulating ($\mathbf{n} \cdot \nabla \hat{\varphi} = 0$, \mathbf{n} is the normal to the wall); all the other boundaries are assumed to be perfectly conducting ($\hat{\varphi} = 0$). Nonslip condition is applied to all walls.

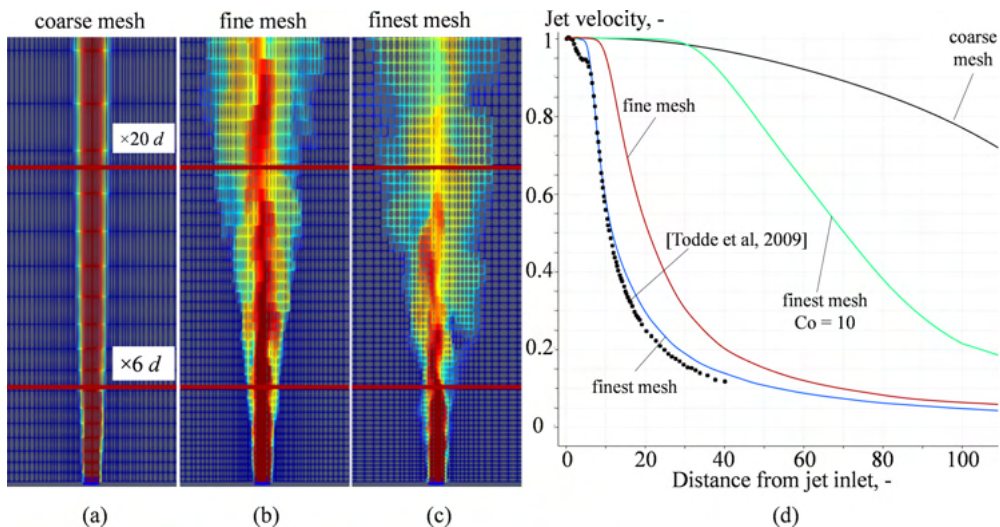


FIG. 3. Study of mesh convergence at $Re = 2700$. Details of the (a) coarse, (b) fine, and (c) finest meshes are colored with the jet velocity; (d) comparison of the simulation results with the experiment from Todde *et al.* [22]. Cell size is variable; in the breakup zone ($Z < 100d$) there are, respectively, 38, 85, and 106 cells for the coarse, fine, and finest mesh.

III. RESULTS

A. Non-MHD jet and mesh study

Since the domain is very large, one has to pay attention to the resolution of the grid along the jet axis and near the walls to correctly track the hydrodynamic and induced current. The

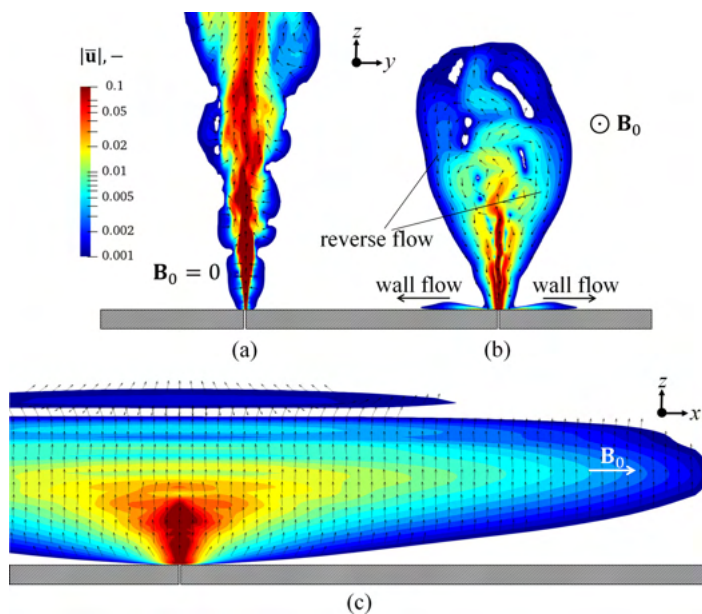


FIG. 4. Instantaneous velocity magnitude of a turbulent free jet ($Re = 2700$) (a) without magnetic field ($N = 0$); (b), (c) with magnetic field ($N = 0.1$).

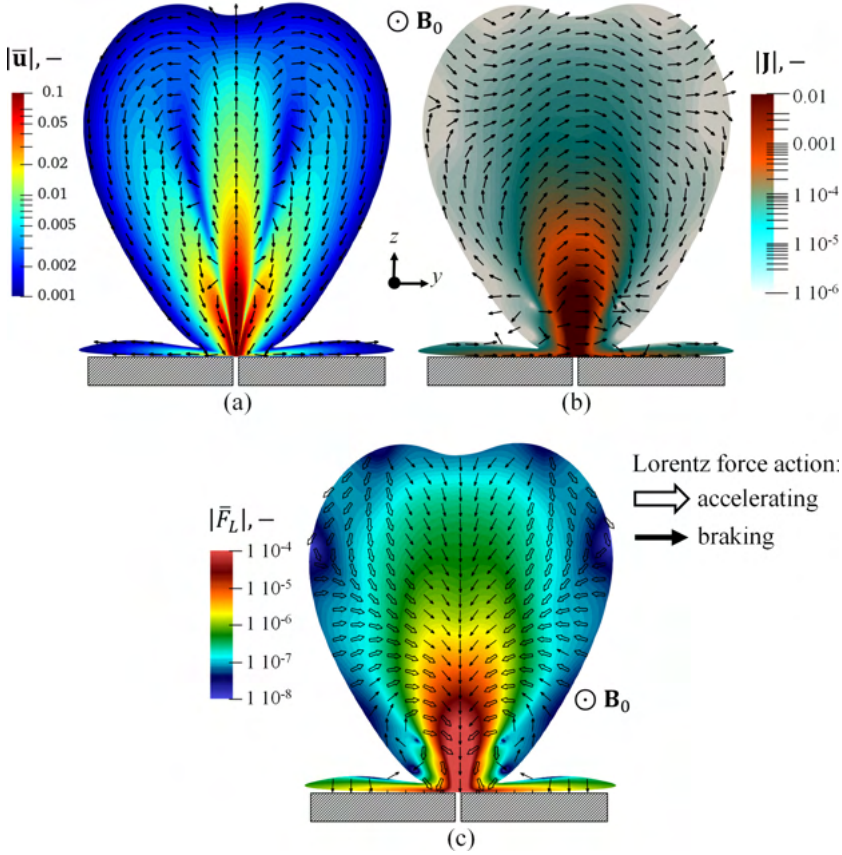


FIG. 5. Time-averaged jet structure in central vertical plane normal to magnetic field for the case $Re = 2700$ and $N = 0.1$: (a) velocity field; (b) induced current density; (c) Lorentz force. Vectors show the direction of the corresponding field. Thick arrows indicate acceleration and common arrows mean braking of the flow by the Lorentz force.

jet flow experiment performed by Todde *et al.* [22] for Reynolds numbers of 2700 was used to verify the simulation results without magnetic field and to perform the mesh resolution studies (see Fig. 3). Since most decay happens for the vertical positions Z between 6 and 20 inlet diameters [Fig. 3(d)], this region should be significantly refined. To save computational time, and due to the large extension of the calculation domain [Fig. 2(a)], nonuniform meshes were used.

Three nonuniform meshes using (a) coarse 5×10^5 , (b) fine 10^6 , and (c) very fine 6.5×10^6 mesh elements were tested. Sensitivity to time integration was also done by varying the Courant number (Co) from 0.1 up to a value of 10. Good results with the very finest mesh were achieved with a reasonable calculation time using Co of 0.5. Using higher Courant numbers generates incorrect integration in time, which leads to unphysical results by strongly delaying the jet decay (see results for $Co = 10$). The numerical solution correctly reproduces the experimental data only for the finest mesh. Thereby the finest mesh and Co of 0.5 will be used for the MHD study.

B. MHD jet

The presented study concerns the Reynolds numbers (850; 2700; 4050) and interaction numbers (0.01; 0.05; 0.1). For all these conditions, the jet flow and its induced currents are highly transient. The main characteristics are better seen after time averaging. We present in more detail the

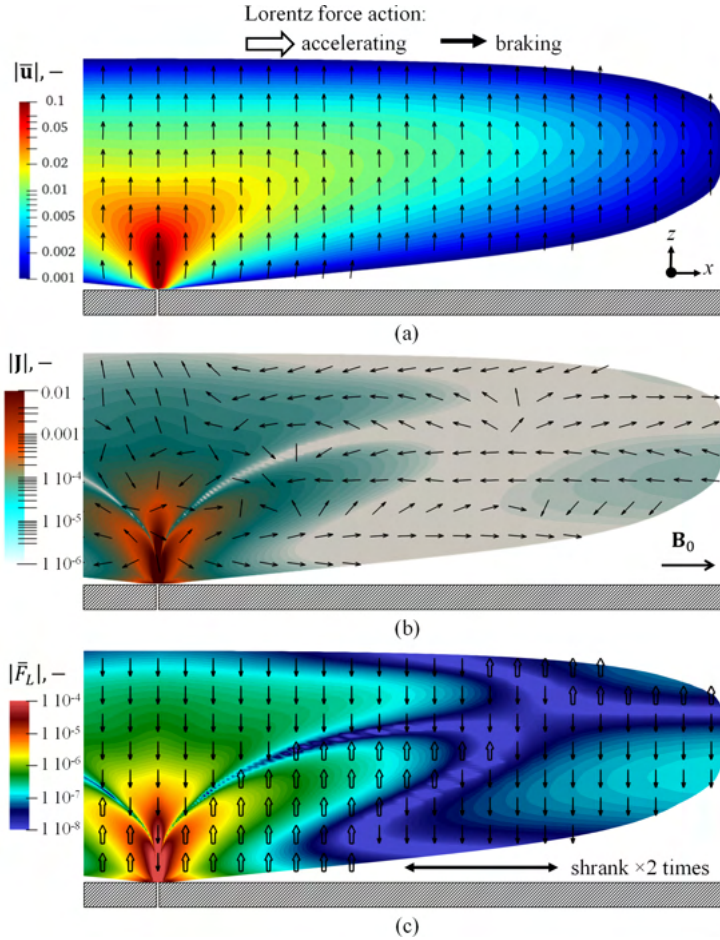


FIG. 6. Time-averaged jet structure in central vertical plane parallel to magnetic field for the case $Re = 2700$ and $N = 0.1$: (a) velocity field; (b) induced current density; (c) Lorentz force. Vectors show the direction of the corresponding field. Thick arrows indicate acceleration and common arrows mean braking of the flow by the Lorentz force. Geometry is compressed two times in the magnetic field direction.

case $Re = 2700$ and $N = 0.1$ ($Ha \sim 16.5$). The non-MHD turbulent jet ($N = 0$) was found to develop symmetrically in all directions; the expansion is controlled by the lateral momentum fluxes transported by turbulent eddies (Fig. 4). When the transverse magnetic field $N = 0.1$ is introduced, the jet loses some of its length and symmetry. It extends preferentially in the direction of the magnetic field (Figs. 4–8). The two reverse-flow zones predicted by Davidson [14] are clearly visible at immediate vicinity of the main jet. Due to their high-velocity magnitude, these two reverse flows can also be qualified as jet. These jets hit the bottom boundary and generate horizontal outward wall flows [Figs. 4(b) and 5(a)]. The key to understand this flow structure is to look at the development of the current distribution (Figs. 4–6). Induced current generated within the jet core ($\hat{u} \times \hat{B}$) must form closed paths, which close mainly in the plane perpendicular to the jet sheet (Fig. 7). The current paths adopt the characteristic dipolelike structure, with the induced current returning through regions far from the jet core. In the present case except at the close vicinity of the inlet, due to the extension of the jet (Fig. 7), most of the electric current lines close through the conducting walls.

To understand the origin of the jet flattening and reverse flows, it is necessary to look at the Lorentz force distribution (Figs. 5 and 6), which is a direct result of the electric current lines distribution.

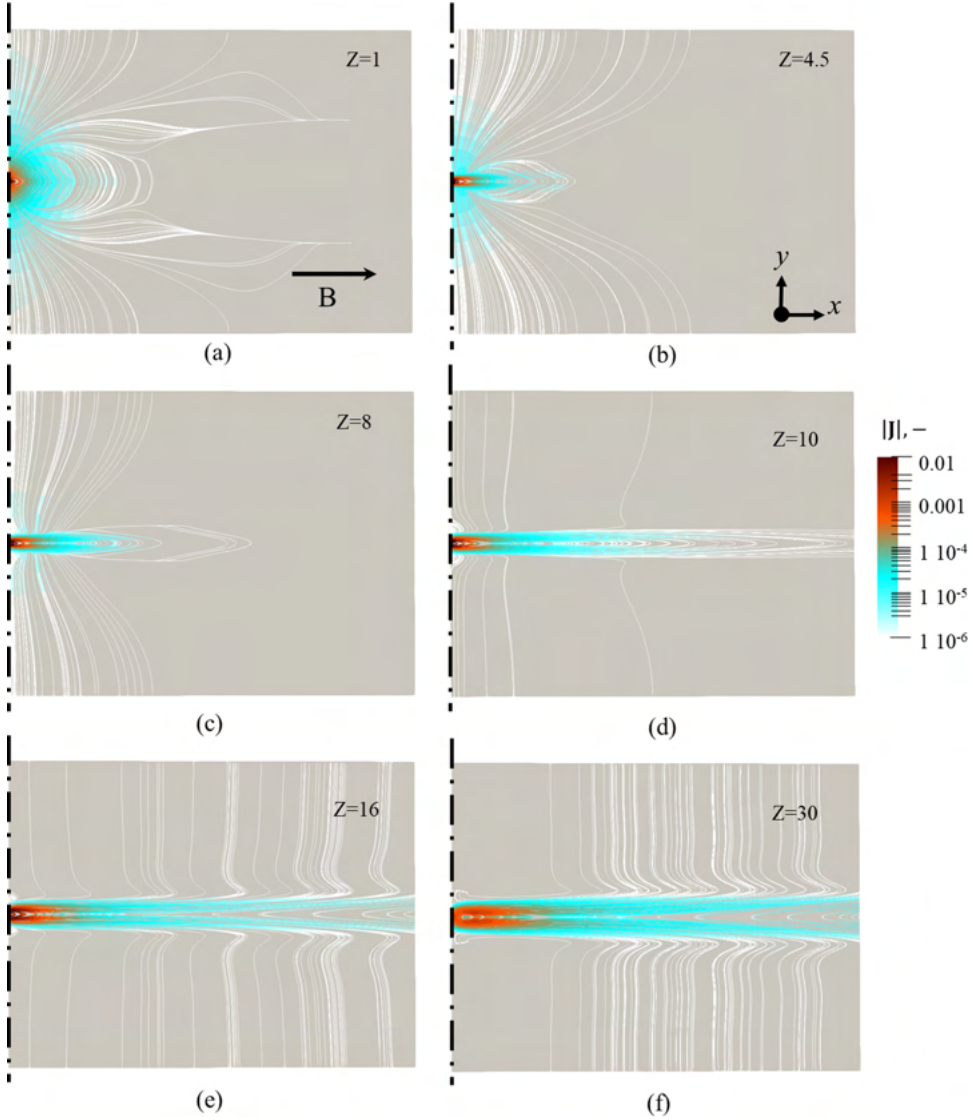


FIG. 7. Time-averaged horizontal distribution of the induced electric current lines for $Re = 2700$ and $N = 0.1$ at different height. For the sake of clarity geometry is compressed in the magnetic field direction and only half plane is shown ($X > 0$).

Depending on the sign of the scalar product $\Psi = \text{sgn}(\mathbf{u} \bullet \mathbf{F}_L)$ the Lorentz forces acts as braking or an accelerating force:

$$\Psi = \begin{cases} -1 & \text{for } \mathbf{u} \bullet \mathbf{F}_L < 0; \\ 0 & \text{for } \mathbf{u} \bullet \mathbf{F}_L = 0; \\ 1 & \text{for } \mathbf{u} \bullet \mathbf{F}_L > 0 \end{cases} \quad (11)$$

The Lorentz force brakes [Figs. 5, 6, 8, and 9(c)] the jet core. However, almost everywhere else, the Lorentz force accelerates the fluid. In the direction along the magnetic field, the Lorentz force acts in the upward direction, i.e., in the direction of the jet. This explains why the jet develops a thin sheetlike structure (Figs. 7 and 8). In the direction perpendicular to the magnetic field, the

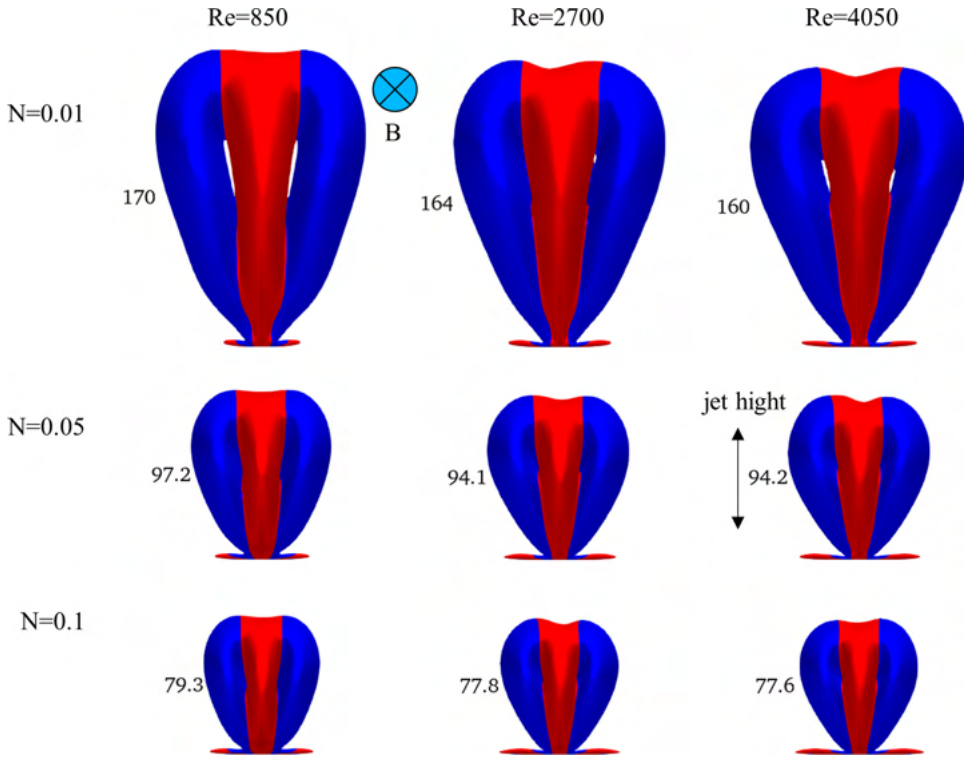


FIG. 8. Time-averaged jet shape in the normal to the magnetic field plane based on the Reynolds and interaction numbers. The color indicates braked ($\Psi = -1$, red) and accelerated ($\Psi = +1$, blue) region by the Lorentz force. The jet isosurface corresponds to the velocity magnitude of 0.001. Numbers next to jet indicate its dimensionless height in inlet diameters (d). The jet height and “thickness” seem to depend solely on N .

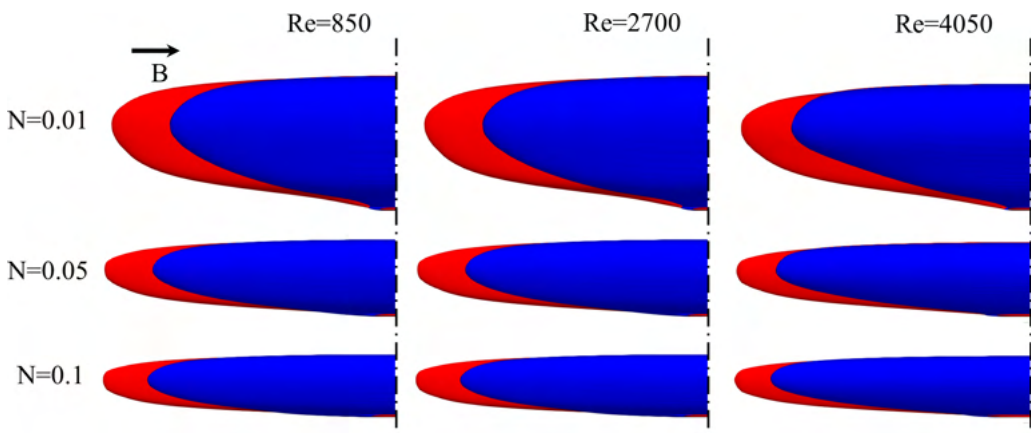


FIG. 9. Time-averaged jet shape in the parallel to the magnetic field plane based on the Reynolds and interaction numbers. The jet isosurface corresponds to the velocity magnitude of 0.001. The color indicates braked ($\Psi = -1$, red) and accelerated ($\Psi = +1$, blue) region by the Lorentz force.

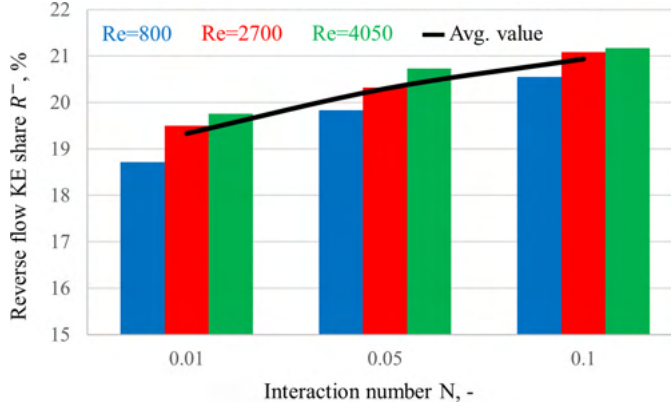


FIG. 10. Time-averaged reverse flow kinetic energy (KE) share R^- [Eq. (12)] for Reynolds numbers 850, 2700, 4050 vs the interaction number.

Lorentz force acts on a region which would have been relatively stagnant in the non-MHD case. However, the direction of the Lorentz force is now “downward,” i.e., the direction opposite to the jet. It results in the development of the reverse-flow zones, adjacent to the thin elongated jet flowing upward. Velocity magnitudes in the reverse region are almost as strong as within the jet. The two reverse-flow regions stick to the jet, and hit the bottom wall at very close distance from the jet inlet. This allows the development of strong flow recirculation loops [Fig. 5(a)], which resembles a 2D fountain (Figs. 5, 6, 8, and 9). Local braking and acceleration results in a redistribution of the momentum along the magnetic field by means of electromagnetics. All the time-averaged results confirm fully the theoretical prediction made by Davidson [14,23].

To estimate the percentage of the kinetic energy (KE) contained in the reverse flow R^- in the simulated MHD jet, the following expression was used:

$$R^- = \frac{\Phi^-}{\Phi^+ + \Phi^-} \times 100\%, \quad (12)$$

where Φ^+ and Φ^- represent a volume integral of the KE of the axial time-averaged velocity component u_z in the aligned or opposite direction to the main jet:

$$\Phi^+ = \int \hat{u}_z^2 H(\hat{u}_z > 0) dV \quad \text{and} \quad \Phi^- = \int \hat{u}_z^2 H(-\hat{u}_z > 0) dV, \quad (13)$$

where $V(x,y,z)$ is the computational cell volume and H the Heaviside step function. As one can see from Fig. 10, the reverse flow kinetic energy part represents (~ 18 – 22%) and depends more on the interaction number than on the Reynolds number.

The instantaneous results show the presence of flow and electric current coherent structures (Figs. 11 and 12). The two opposite adjacent flows promote the development of vortices aligned with the applied magnetic field (Fig. 11). These vortices originate near the inlet where jet and reversed flows are at their highest magnitude. They are generated by a Kelvin-Helmholtz instability at the shear boundary between the main jet and its adjacent reverse jet sheets [2,24]. Misaligned vortices are reoriented by the Lorentz force in the magnetic field direction. In Fig. 11 it can be seen how bended vortical structures at the jet inlet become progressively horizontally aligned with the magnetic field [16,25].

The presence of these coherent vortical structures drifting upward is associated with intense induced current (Fig. 12). The antisymmetric organization of the large-scale vortices induce a stratification of induced electric current [Fig. 12(b)]. Parallel to \mathbf{B} , these stratified currents have components oscillating from left to right resulting from the closure of the horizontal currents traveling through vortices with opposite vorticity (Fig. 11).

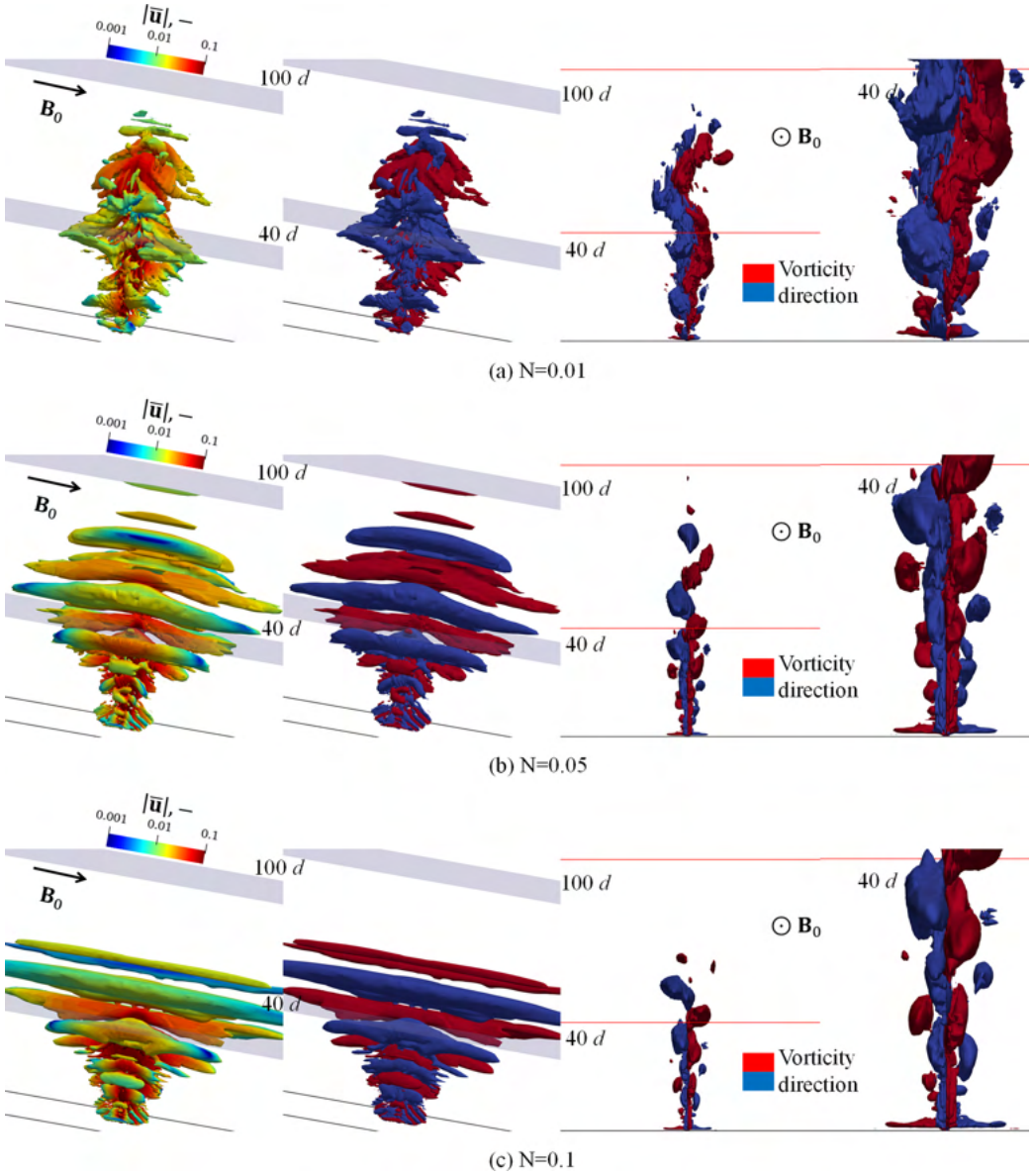


FIG. 11. Instantaneous vortical structure (Q criterion with $Q = 5 \times 10^{-6}$) for $Re = 2700$ for different $N = 0.01, 0.05, 0.1$. Additionally, results in the form of videos for $N = 0.05$ for $Re = 4050$ and $Re = 850$ can be found in the Supplemental Material [26].

C. Damping of the jet under magnetic field

Assuming a limitless domain, the damping of axial velocity was derived theoretically in Ref. [23] as

$$u_z \sim \left(\frac{\tau M^2}{L_0^4 z} \right)^{1/3}, \quad (14)$$

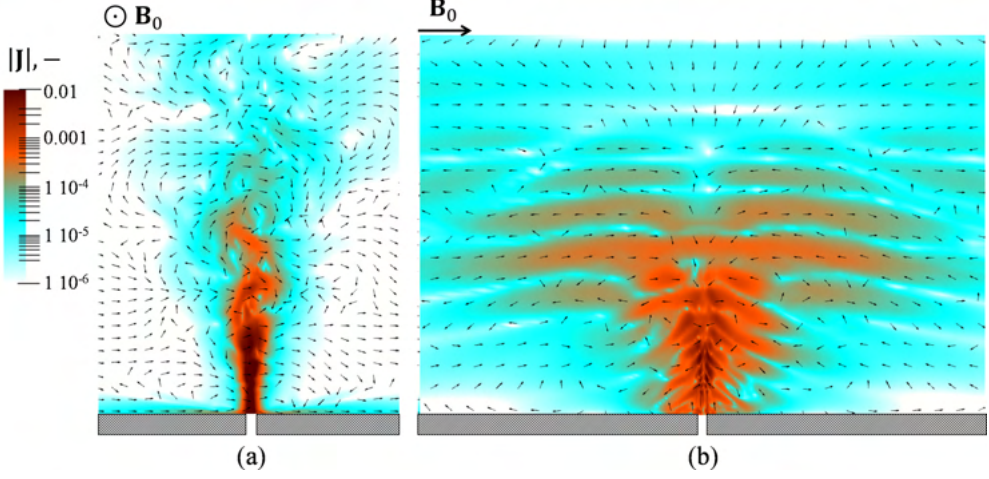


FIG. 12. Instantaneous induced electric current density \mathbf{J} distribution in (a) normal and (b) parallel planes to the applied magnetic field ($Re = 2700$, $N = 0.1$). Additionally, results in the form of videos for $N = 0.05$ for $Re = 4050$ and $Re = 850$ can be found in the Supplemental Material [26].

where τ is the Joule damping time: $\tau = (\frac{\sigma_0 \mathbf{B}_0^2}{\rho})^{-1}$ and M represents the axial momentum at the inlet:

$$M = const = \int \hat{u}_z^2 dA = U_0^2 \frac{\pi L_0^2}{4}, \quad (15)$$

where $A(z)$ is the domain cross section. In the dimensionless form, Eq. (14) becomes

$$\hat{u}_z \sim \left(\frac{\pi^2}{16} \frac{1}{Nz} \right)^{1/3}. \quad (16)$$

The first consequence is that the volume of the jet defined by a specific velocity magnitude depends solely on the interaction number \mathcal{N} (Figs. 8 and 9). Indeed, the jet perfectly keeps its height and length for the equal interaction numbers; the shape slightly differs, e.g., for lower Reynolds numbers it is of a “bulky” shape.

A quantitative comparison of Eq. (16) with the simulated jet decay is presented in Fig. 13. It can be observed that for all studied cases, the MHD jet decays faster than the hydrodynamic jet ($N = 0$). The decay is stronger for higher N [see Figs. 13(a)–13(c)]. The agreement is good within a limited distance from the inlet. At larger distance, the jet decays much faster than predicted by Eq. (16). The reason lies in the closure of the currents inside a limited domain. At these distances the jet elongation reached the vicinity of the outer boundary of our calculation domain [Fig. 7(d)]. An important part of the induced currents lines cross through the walls. The accelerating portion of the Lorentz force which was responsible for the jet elongation is now acting virtually beyond the walls. The assumption leading to Eq. (16) does not hold anymore for Z positions where current closes through the walls. As an example we can compare Figs. 13(b) and 7 for $Re = 2700$ and $N = 0.1$., where the limit in validity of Eq. (16) can directly be related to the closure of currents through the walls, occurring at $Z > 8$. For higher Z , since the propagation of linear momentum along the field lines is hindered, Joule dissipation cannot be reduced. The magnetic field action reduces to almost a braking effect. In these conditions, an equilibrium between viscous and Lorentz forces can be assumed. The decay must thus follow:

$$\hat{u}_z \sim e^{-\sqrt{N}z}. \quad (17)$$

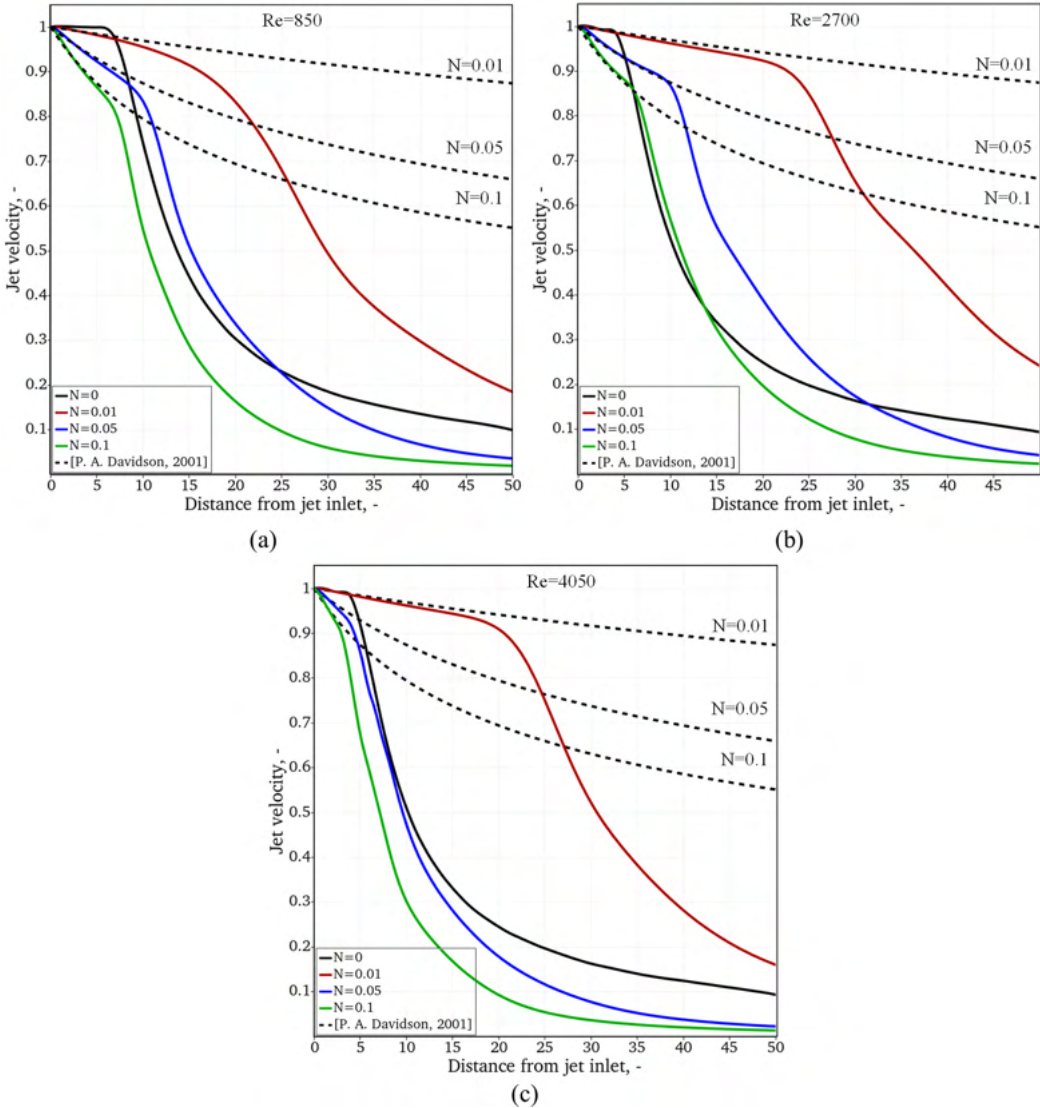


FIG. 13. Normalized jet destruction function compared to Ref. [23] [dashed lines, Eq. (16)] and simulated jet damping for the undisturbed jet (black) and under applied magnetic field (colored) for the Reynolds numbers (a) 850; (b) 2700; (c) 4050.

This exponential decay describes well the much faster decay [compared to Eq. (16)] observed at larger distances from the jet inlet (Fig. 13).

It is interesting to see how the closure of electric current at a distances of $800d$ can affect the jet decay. While the present study uses perfectly conducting side walls, insulating wall boundaries conditions would give rise to Hartmann and side layers. Based on literature data, additional instabilities could possibly affect the jet and the boundary layers [3,5,20,25].

IV. CONCLUSIONS

The application of a transverse magnetic field is often reduced to a damping or smearing effect. The present study shows that an inlet round jet undergoes an anisotropic flattening along

the magnetic field direction, while two reverse jet flow zones develop adjacent to the main jet. These results show clearly that the momentum redistributed by the electromagnetic field cannot be fully explained either with a “porous media” or with a viscous stress increase similarity. The full understanding can only be achieved by considering the loops made by the induced electric current. The jet dynamics and decay rate was found to be sensitive to external electrical boundary conditions even at very large distances ($\sim 800d$). The apparition of strong vortical structures raises the question on the actual turbulence damping. In the present configuration the MHD does not seem to extinguish the turbulence but rather transform it into another anisotropic form. These large and powerful vortices could possibly result from a spectral momentum transfer from the small “damped” scales by a mechanism of inverse cascade. However, in the present case we rather incline towards a simpler Kelvin-Helmholtz instability mechanism. Evolution of turbulence and effects of external electrical boundary conditions in such configurations deserve further studies.

ACKNOWLEDGMENTS

The authors acknowledge the financial support by the Austrian Federal Ministry of Economy, Family and Youth and the National Foundation for Research, Technology and Development within the framework of the Christian Doppler Laboratory for Metallurgical Applications of Magnetohydrodynamics.

-
- [1] I. Contopoulos, Electric currents along astrophysical jets, *Galaxies* **5**, 71 (2017).
 - [2] L. Bühler, T. Arlt, T. Boeck, L. Braiden, V. Chowdhury, D. Krasnov, C. Mistrangelo, S. Molokov, and J. Priede Magnetically induced instabilities in duct flows, *IOP Conf. Ser.: Mater. Sci. Eng.* **228**, 012003 (2017).
 - [3] K. Timmel, S. Eckert, G. Gerbeth, F. Stefani, and T. Wondrak, Experimental modeling of the continuous casting process of steel using low melting point metal alloys-the LIMMCAST Program, *ISIJ Int.* **50**, 1134 (2010).
 - [4] Z. Liu, M. Wu, A. Vakhrushev, M. Wu, E. Karimi-Sibaki, A. Kharicha, A. Ludwig, and B. Li, Scale-adaptive simulation of transient two-phase flow in continuous-casting mold, *Metals* **8**, 609 (2018).
 - [5] A. Vakhrushev, A. Kharicha, Z. Liu, M. Wu, A. Ludwig, G. Nitzl, Y. Tang, G. Hackl, and J. Watzinger, Electric current distribution during electromagnetic braking in continuous casting, *Metall. Mater. Trans. B* **51**, 2811 (2020).
 - [6] A. Vakhrushev, A. Kharicha, E. Karimi-Sibaki, M. Wu, A. Ludwig, G. Nitzl, Y. Tang, G. Hackl, J. Watzinger, and S. Eckert, Generation of reverse meniscus flow by applying an electromagnetic brake, *Metall. Mater. Trans. B* **52**, 3193 (2021).
 - [7] L. Bühler, C. Mistrangelo, and H.-J. Brinkmann, Experimental investigation of liquid metal MHD flow entering a flow channel insert, *Fusion Eng. Des.* **154**, 111484 (2020).
 - [8] M. Sajben and J. A. Fay, Measurement of the growth of a turbulent mercury jet in a coaxial magnetic field, *J. Fluid Mech.* **27**, 81 (1967).
 - [9] M. Ievlev and V. B. Levin, Laminarization of submerged jet of electrically conducting fluid by means of a longitudinal magnetic field, *Fluid Dyn.* **24**, 851 (1989).
 - [10] P. Hoult, Turbulent mercury jets, *Phys. Fluids* **10**, 2345 (1967).
 - [11] S. Preobrazhenskii and I. A. Chinenkov, Experimental investigation of the effect of a longitudinal magnetic field on turbulent jets of a conducting fluid, *Magnetohydrodynamics* **6**, 208 (1970).
 - [12] Y. Kolesnikov, D. Krasnov, and T. Boeck, Evolution of a round jet in a duct in the presence of a uniform axial magnetic field, *Magnetohydrodynamics* **53**, 119 (2017).
 - [13] D. Krasnov, Y. Kolesnikov, and T. Boeck, Numerical simulation of electrically conducting jet flow in a straight duct under longitudinal homogeneous magnetic field, *Phys. Fluids* **31**, 014108 (2019).
 - [14] P. A. Davidson, Magnetic damping of jets and vortices, *J. Fluid Mech.* **299**, 153 (1995).

- [15] A. Alemany, R. Moreau, P. L. Sulem, and U. Frisch, Influence of an external magnetic field on homogeneous MHD turbulence, *J. Fluid Mech.* **18**, 277 (1979).
- [16] R. Moreau and A. Alemany, *Experimental results on MHD homogeneous turbulence*, in *Structure and Mechanisms of Turbulence II*, Lect. Notes Phys.76, edited by H. Fiedler (Springer, Berlin, 1978).
- [17] L. Bühler, H.-J. Brinkmann, and C. Mistrangelo, Experimental investigation of liquid metal pipe flow in a non-uniform magnetic field, *Magnetohydrodynamics* **56**, 131 (2020).
- [18] H. Harada, K. Okazawa, M. Tanaka, and E. Takeuchi, in *Proceedings of the International Symposium on Electromagnetic Processing of Materials, EPM'94* (Nagoya University, Nagoya, Japan, 1994).
- [19] F. Nicoud and F. Ducros, Subgrid-scale stress modelling based on the square of the velocity gradient tensor, *Flow Turbul. Combust.* **62**, pp. 183 (1999).
- [20] R. Chaudhary, C. Ji, B. G. Thomas, and S. P. Vanka, Transient turbulent flow in a liquid-metal model of continuous casting, including comparison of six different methods, *Metall. Mater. Trans. B* **42**, 987 (2011).
- [21] H. Kobayashi, Large eddy simulation of magnetohydrodynamic turbulent channel flows with local subgrid-scale model based on coherent structures, *Phys. Fluids*. **18**, 045107 (2006).
- [22] V. Todde, P. G. Spazzini, and M. Sandberg, Experimental analysis of low-Reynolds number free jets, *Exp. Fluids* **47**, 279 (2009).
- [23] P. A. Davidson, *Introduction to Magnetohydrodynamics* (Cambridge University Press, Cambridge, 2001).
- [24] Y. Laghouati, A. Bouabdallah, M. Zizi, and A. Alemany, MHD Kelvin-Helmholtz instability in non-hydrostatic equilibrium, *J. Phys. Conf. Ser.* **64**, 012010 (2007).
- [25] V. Chowdhury, L. Bühler, C. Mistrangelo, and H.-J. Brinkmann, Experimental study of instabilities in magnetohydrodynamic boundary layers, *Fusion Eng. Des.* **98–99**, 1751 (2015).
- [26] See Supplemental Material at <http://link.aps.org/supplemental/10.1103/PhysRevFluids.6.123701> for results in the form of videos for $N = 0.05$ for $Re = 405$ and $Re = 850$.